PHYSICAL REVIEW B **84**, 134525 (2011)

Combined effects of pressure and Ru substitution on $BaFe_2As_2$

S. K. Kim,[1,2] M. S. Torikachvili,[2,3] E. Colombier,[1] A. Thaler,[1,2] S. L. Bud'ko,[1,2] and P. C. Canfield[1,2]

[1]*Ames Laboratory, Iowa State University, Ames, Iowa 50011, USA*

[2]*Department of Physics and Astronomy, Iowa State University, Ames, Iowa 50011, USA*

[3]*Department of Physics, San Diego State University, San Diego, California 92182, USA*

(Received 28 July 2011; revised manuscript received 19 September 2011; published 18 October 2011)

The *ab* plane resistivity of $Ba(Fe_{1-x}Ru_x)_2As_2$ ($x = 0.00$, 0.09, 0.16, 0.21, and 0.28) was studied under nearly hydrostatic pressures, up to 7.4 GPa, in order to explore the $T - P$ phase diagram and to compare the combined effects of isoelectronic Ru substitution and pressure. The parent compound $BaFe_2As_2$ exhibits a structural/magnetic phase transition near 134 K. At ambient pressure, progressively increasing Ru concentration suppresses this phase transition to lower temperatures at an approximate rate of ~5 K/% Ru correlated with the emergence of superconductivity. By applying pressure to this system, a similar behavior is seen for each concentration: the structural/magnetic phase transition is further suppressed and superconductivity induced and ultimately, for larger x Ru and P, suppressed. A detailed comparison of the $T - P$ phase diagrams for all Ru concentrations shows that 3 GPa of pressure is roughly equivalent to 10% Ru substitution. Furthermore, due to the sensitivity of $Ba(Fe_{1-x}Ru_x)_2As_2$ to pressure conditions, the melting of the liquid media, 4 : 6 light mineral oil : *n*-pentane and 1 : 1 isopentane : *n*-pentane, used in this study could be readily seen in the resistivity measurements. This feature was used to determine the freezing curves for these media and to infer their room temperature, hydrostatic limits: 3.5 and 6.5 GPa, respectively.

DOI: 10.1103/PhysRevB.84.134525 PACS number(s): 74.62.Fj, 74.70.Xa, 75.30.Kz, 74.10.+v

I. INTRODUCTION

Many studies have investigated the effects of electron, hole, and isovalent substitutions in the $AEFe_2As_2$ (AE = alkaline earth) system.[1–11] For $BaFe_2As_2$, in some cases this substitution causes the suppression of the structural/magnetic transition temperature (T_{sm}) and the emergence of superconductivity.[1–7] In other cases, such as substitution of Cr or Mn for Fe, T_{sm} is suppressed without superconductivity ever stabilizing.[5,9] For the case of $Ba(Fe_{1-x}Ru_x)_2As_2$, increasing the concentration of isovalent Ru (Ref. 11) reveals behavior similar to Co substitution[6] but without introducing additional charge carriers into the system.[11,12] Pressure has also been used as an isoelectronic tuning mechanism.[13–21] As pressure is applied to these systems, T_{sm} is suppressed gradually and disappears at a critical pressure P_{crit}. The superconducting temperature (T_c) reaches its maximum value and the transition width is narrowest near P_{crit}.[13,22]

Although Ru substitution for Fe gives rise to an increase of the unit cell volume, the *c*-lattice parameter and the ratio of the *c*-lattice parameter to the *a*-lattice parameter (*c*/*a*) both decrease with increasing Ru concentration.[11] Using pressure-dependent crystallographic data for $BaFe_2As_2$,[23] it was shown by Thaler *et al.*[11] that the ambient pressure $T - x$ phase diagram for $Ba(Fe_{1-x}Ru_x)_2As_2$ and $T - P$ phase diagram for $BaFe_2As_2$ manifest similar features and can be scaled to each other[11] by creating a T versus *c*/*a* phase diagram. This scaling is not universal, though: for $BaFe_2(As_{1-x}P_x)_2$, T_{sm} and T_c scale better with changes in c than with changes in *c*/*a*.[11] In order to better quantify and understand the similarities between the effects of Ru substitution and pressure, we have determined the $T - P$ phase diagrams for multiple Ru substitution levels and explored the possibility of a universal scaling between these isoelectronic tuning mechanisms.

In addition, it is well known that the behavior of $BaFe_2As_2$ is sensitive to pressure conditions.[13–16] Pressure inhomogeneities associated with nonhydrostatic conditions tend to decrease the pressure needed to suppress T_{sm} and induce superconductivity. This sensitivity causes discrepancies in the construction of the $T - P$ phase diagram. Therefore, conditions as close to hydrostatic as possible are necessary for consistent results. In this study a piston-cylinder cell and a modified Bridgman cell with appropriate liquid media were used to measure the resistivity of $Ba(Fe_{1-x}Ru_x)_2As_2$ samples under pressure. A maximum pressure of 7.4 GPa was achieved. Although parent $BaFe_2As_2$ has already been measured several times under various pressure conditions,[13–17] it was measured again under the same conditions as the $Ba(Fe_{1-x}Ru_x)_2As_2$ samples in order to allow for more reliable comparisons as well as to gauge the level of hydrostaticity of the liquid medium. We find a remarkably simple scaling between pressure and Ru substitution: 3 GPa of applied pressure affects the phase diagram in a manner similar to 10% Ru substitution for Fe.

II. EXPERIMENTAL METHODS

All $Ba(Fe_{1-x}Ru_x)_2As_2$ single crystals measured in this study were grown out of self-flux using the method described by Thaler *et al.*[11]

Electrical resistivity measurements under pressures of up to 2.3 GPa were conducted using a piston cylinder pressure cell.[18,19] Higher pressures, up to 7.4 GPa, were achieved using a Bridgman cell that was modified to work with liquid pressure media.[24] Both these cells were designed to fit inside a Quantum Design Physical Properties Measurement System (PPMS) which served as a variable-temperature station for the temperature range between 1.8 and 300 K.

The piston-cylinder cell has a Be-Cu body with a center core made out of tungsten carbide. The samples for this cell were cut into rectangles with dimensions of approximately $1.5 \times 0.3 \times 0.1$ mm^3. Four Pt wires were attached to the

sample using Epotek H20E silver epoxy. The feedthrough containing the sample, Manganin, and Pb manometers was inserted in a polytetrafluoroethylene cup containing a 4 : 6 mixture of light mineral oil and *n*-pentane, which served as the liquid pressure-transmitting medium, unless otherwise stated. Pressure was applied at ambient temperature with a hydraulic press using the Manganin as a reference manometer. A calibrated Cernox sensor was attached to the body of the cell for temperature measurements. At low temperatures the pressure was determined from the superconducting temperature T_c of the Pb manometer.[25] The cooling and warming rates were kept below 0.5 K/min, which corresponded to a temperature lag between the sample and Cernox sensor of less than 0.5 K at high temperatures and less than 0.1 K for temperatures less than 70 K. Further details are already described elsewhere.[19] Cooling data are shown in this work unless otherwise stated.

The modified Bridgman cell has a Be-Cu body with opposing, nonmagnetic, tungsten-carbide anvils. A 1 : 1 mixture of isopentane : *n*-pentane was used as the liquid pressure-transmitting medium. Although we determined that this liquid medium has a higher hydrostatic limit of 6.5 GPa (hydrostatic limit being defined as the pressure at which the medium begins to solidify at ambient temperature) (see Appendix) than Fluorinert mixtures,[26–29] it also has a higher compressibility, which means lower maximum pressures can be achieved without changes to critical cell dimensions. Moreover, there was a higher rate of failure for the wires within the sample chamber when using the isopentane : *n*-pentane mixture, where a wire within the cell would break or a contact on the sample would be lost. Despite these difficulties, the higher hydrostatic limit made it preferable over other liquid media (e.g., Fluorinert mixtures with hydrostatic limits in the $1-2$ GPa range). For the Bridgman cell, samples were cleaved and cut into approximately $700 \times 150 \times 30\ \mu\text{m}^3$ and four 12.5 μm-diameter gold wires were spot welded onto the sample to create electrical contacts for standard four-probe measurements. The pressure within the cell was determined using the superconducting temperature T_c of Pb.[25] For these cells, the difference between the pressure at room temperature and at low temperature was previously determined to be less than 0.1 GPa.[22] For all Bridgman cell measurements, data were taken while warming from base temperatures. For $T < 35$ K data were taken after the temperature was stabilized at each point, ensuring a minimal thermal gradient between the cell and the sample. For measurements above 35 K, the cell was warmed at a rate of 0.5 K/min, which leads to a maximum temperature lag of approximately 1.2 K.[22] Only warming data are shown in this work.

Due to the small dimensions of the samples used in the Bridgman cell, resistivity values can have errors of up to 50%. Furthermore, the micaceous nature of the crystals makes them prone to exfoliation, a tendency which is compounded by the inevitable damage inflicted by the cleaving and cutting done to shape them into the appropriate dimensions. Great care was taken to choose samples with as few of these defects as possible, but it is possible that under pressure the layers could be compressed or further distorted, leading to changes in the strains in the sample, resulting in small jumps or changes in resistivity values. So as to provide a better view of the evolution of the sample behavior with pressure, the piston cylinder cell data were normalized so that the ambient temperature and pressure resistivity values matched those of the corresponding Bridgman cell sample.

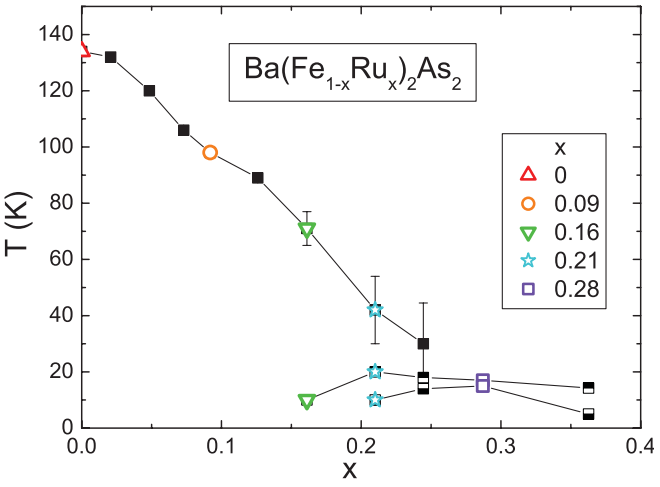

FIG. 1. (Color online) $T-x$ phase diagram for $Ba(Fe_{1-x}Ru_x)_2As_2$.[11] Open symbols indicate the Ru concentrations that were studied under pressure.

Figure 1 shows the $T-x$ phase diagram for $Ba(Fe_{1-x}Ru_x)_2As_2$.[11] The open symbols indicate the Ru concentrations that were chosen for this study in order to explore the low-x and optimal-x regions of the phase diagram. The criteria for T_c are shown in Fig. 2(b). The onset T_c was taken as the intersection of the extrapolated lines seen in the inset of Fig. 2(b). The temperature at which the resistivity reaches zero, as seen in Fig. 2(b), is denoted as $T_{c,\rho=0}$.

Strain-induced, granular or filamentary superconductivity is known to occur in many of the $AEFe_2As_2$ systems.[19,21,30,31] To gauge the impact of this effect on the superconducting phase transition, current-dependent resistivity measurements were done at various pressures. Figure 3 shows two such measurements. At 3.64 GPa [Fig. 3(a)] only the onset of the superconducting transition is seen and there is a definite dependence on the applied current, which suggests that granular or filamentary superconductivity is responsible for the resistance decrease. At 6.21 GPa [Fig. 3(b)] this current dependent behavior is less prominent but still seen during the superconducting transition. The difference in the zero resistivity temperature of the superconducting transition between 0.01 and 1 mA of applied current is ~3 K. Based on the assumption that the effects of granular or filamentary superconductivity will be suppressed by higher current densities, a 1 mA current was used for all measurements.

III. RESULTS

A. $BaFe_2As_2$

Previous pressure measurements of $BaFe_2As_2$ with a modified Bridgman cell have been reported[13,15] using a Fluorinert (FC) mixture of 1 : 1 FC70 and FC77 as the liquid pressure-transmitting medium. The hydrostatic limit for this medium is ~1 GPa;[28] thus an additional, poorly-controlled, small, uniaxial stress component was likely present at higher

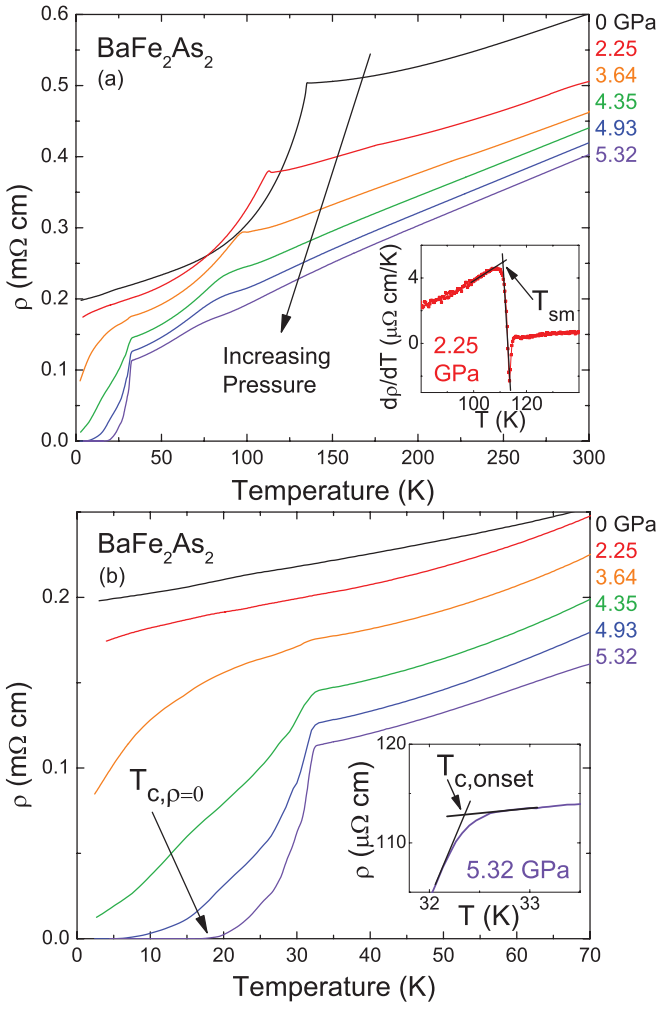

FIG. 2. (Color online) Temperature dependence of the resistivity of $BaFe_2As_2$ for pressures up to 5.32 GPa measured using the modified Bridgman cell. (a) Measurements are shown for temperatures up to 300 K. Inset shows criteria used for the determination of T_{sm}. (b) Same measurements shown for temperatures up to 70 K with criterion used for $T_{c,\rho=0}$. Inset shows the criterion used for $T_{c,onset}$.

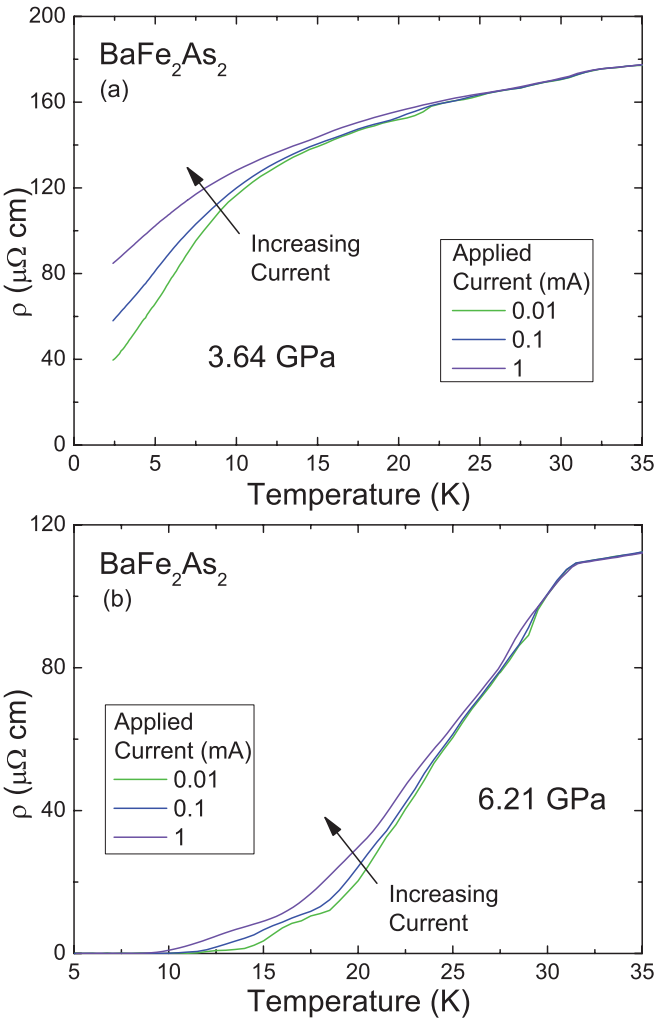

FIG. 3. (Color online) Resistivity measurements of $BaFe_2As_2$ with applied currents of 0.01, 0.1, and 1 mA at (a) 3.64 GPa and (b) 6.21 GPa.

pressures. Due to the sensitivity of $BaFe_2As_2$ to uniaxial stress, a different liquid medium, a 1 : 1 mixture of isopentane : *n*-pentane, with a higher hydrostatic limit of 6.5 GPa (see Appendix) was used in this study.

Two samples of $BaFe_2As_2$ were measured using the Bridgman cell: one measured up to 5.32 GPa (Fig. 2) and the other up to 6.71 GPa (not shown). The ambient pressure resistivity of $BaFe_2As_2$ decreases upon cooling. At ∼134 K, the sample undergoes a structural/magnetic transition where it converts from a high-temperature, tetragonal, paramagnet to a low-temperature, orthorhombic, antiferromagnet. As pressure is applied, the resistivity decreases and the structural/magnetic transition moves to lower temperatures and broadens. In addition, a small downturn arises at low temperature as a precursor to the superconducting transition. This increasingly kinklike feature is reminiscent of the pressure-induced, granular or filamentary, superconducting behavior seen in $SrFe_2As_2$[13] and $CaFe_2As_2$.[19] A current-dependent resistivity measurement at 3.64 GPa [Fig. 3(a)] suggests that superconductivity in a small fraction of the sample, most likely due to internal strains, precedes the occurrence of a more robust superconducting state when $\rho(T)$ is much less sensitive to the excitation current, as shown in Fig. 3(b).

The resistive feature associated with the structural/magnetic transition is gradually suppressed with pressure but still persists at the maximum pressure achieved (6.4 GPa), even with the emergence of a finite $T_{c,\rho=0}$ at ∼5 GPa. The structural/magnetic transition temperatures for $BaFe_2As_2$ were taken as the maximum of the derivative of the resistivity, as seen in the inset of Fig. 2(a). The general form of the phase diagram is not very dependent on the hydrostaticity of the pressure; however, the features in the phase diagram shift toward higher pressure as hydrostaticity is improved.[13–17] The resulting phase diagram for pure $BaFe_2As_2$ using the isopentane : *n*-pentane mixture is shown in Fig. 4. The phase diagrams for the two separate measurements show qualitatively similar behavior, with a quantitative shift of about 1.5 GPa in the transition temperatures at the highest pressures for run 2. Unfortunately, it is these last three highest-pressure data points that are associated with manometer inconsistencies that may be associated with overestimating the actual pressure

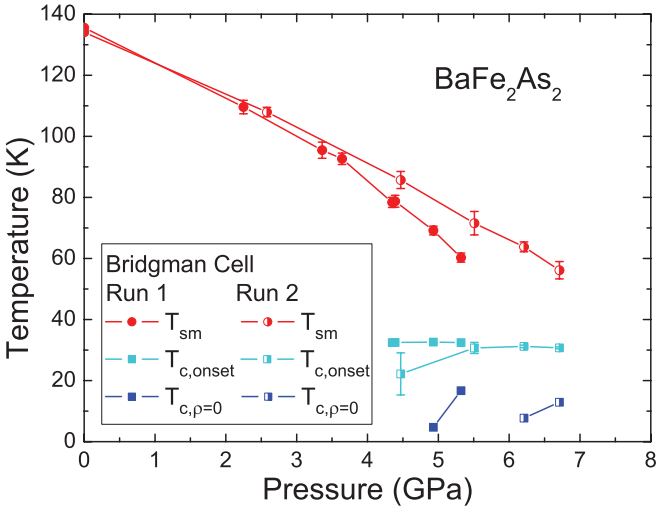

FIG. 4. (Color online) $T - P$ phase diagram for two sets of measurements of $BaFe_2As_2$ using the Bridgman cell. The isopentane : *n*-pentane mixture was used as the liquid pressure-transmitting medium for both measurements.

experienced by the sample. The phase diagram presented in Fig. 4 is in qualitative agreement with previous measurements of $BaFe_2As_2$ under pressure in a Bridgman cell using the Fluorinert mixture[22] but with all transition temperatures shifted to higher pressures for the isopentane : *n*-pentane mixture.

B. $Ba(Fe_{0.91}Ru_{0.09})_2As_2$

As shown in Fig. 4, for pure $BaFe_2As_2$ superconductivity is just being stabilized in the $P \sim 5$ GPa range, while the resistive signature of the structural/magnetic transition remains visible up to our highest measured pressures. For the first Ru concentration in this study we chose $x = 0.09$, which has no bulk superconductivity and an approximately 35 K suppression of T_{sm} (~98 K) from that of the parent $BaFe_2As_2$ ($T_{sm} =$ 134 K).

Two samples of $Ba(Fe_{0.91}Ru_{0.09})_2As_2$ were measured: one with the piston cylinder cell up to 1.83 GPa and another with the Bridgman cell up to 4.94 GPa (Fig. 5). Figure 5 shows the effects of pressure on the resistivity of $Ba(Fe_{0.91}Ru_{0.09})_2As_2$ samples.

With increasing pressure T_{sm} is gradually suppressed to lower temperatures and granular or filamentary superconductivity develops and gradually shorts out more of the sample. When zero resistivity is achieved, with 3.16 GPa of pressure a small feature due to the structural/magnetic transition can still be observed, suggesting that the suppression of the structural/magnetic transition is not complete. Further pressure increase almost completely suppressed the transition and increased $T_{c,\rho=0}$ to a value of 25.7 K at $P_{crit} = 4.94$ GPa. The superconducting transition width also decreased with pressure. At this critical pressure there is no measurable current dependence of the resistivity curve, suggesting the development of bulk superconductivity. As will be seen for higher Ru substitutions, these features are consistent with $P_{crit} \approx 5$ GPa for this sample.

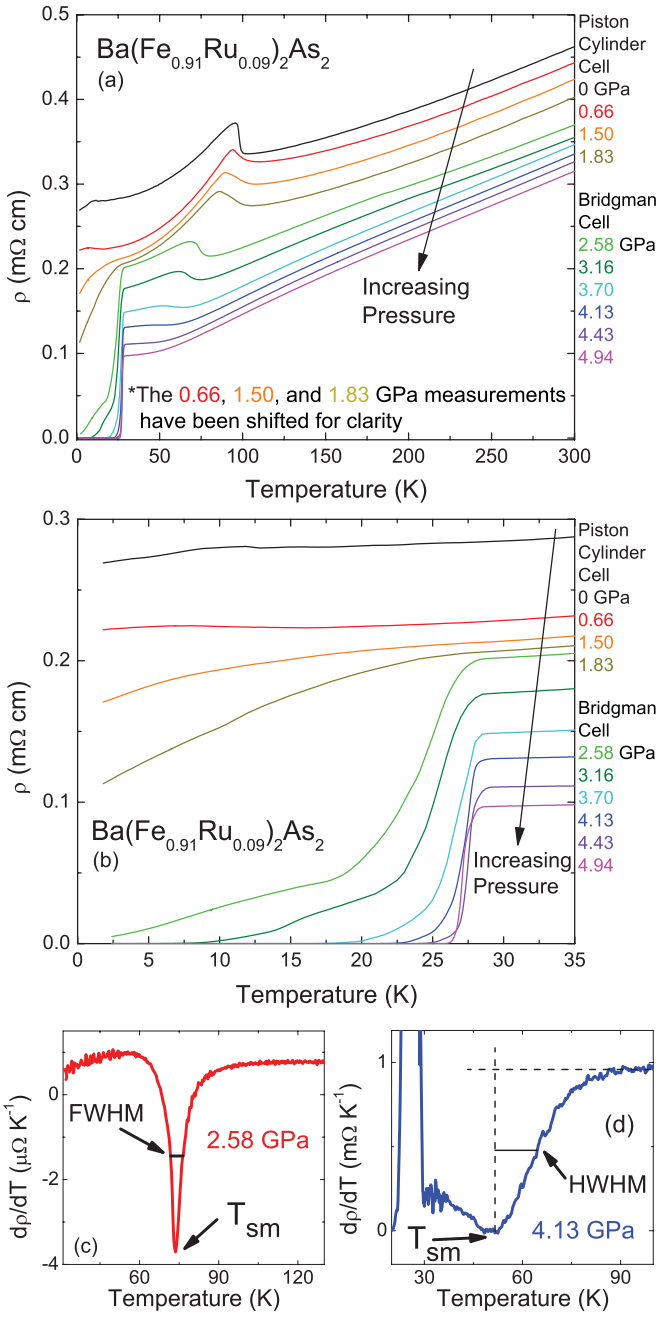

FIG. 5. (Color online) Temperature dependence of the resistivity of $Ba(Fe_{0.91}Ru_{0.09})_2As_2$ up to 1.83 and 4.94 GPa using a piston cylinder cell and a Bridgman cell, respectively. (a) Shown for temperatures up to 300 K. The 0.66, 1.50, and 1.83 GPa measurements have been shifted down by 0.035, 0.045, and 0.06 mΩ cm, respectively, for clarity. (b) Shown for temperatures up to 35 K. (c) and (d) Criteria used to determine T_{sm} and their corresponding error bars.

A phase diagram constructed from these measurements can be seen in Fig. 6. For all Ru-substituted samples measured, T_{sm} was taken as the minimum of the resistivity derivative. Error bars were taken as the full width at half maximum where possible, typically when the structural/magnetic transition was far removed from the superconducting transition. When $T_c \lesssim T_{sm}$ and effectively truncates the lower-temperature part of the $d\rho/dT$ curve, twice the half width at half maximum was used. An example of these criteria can be seen in Figs. 5(c)

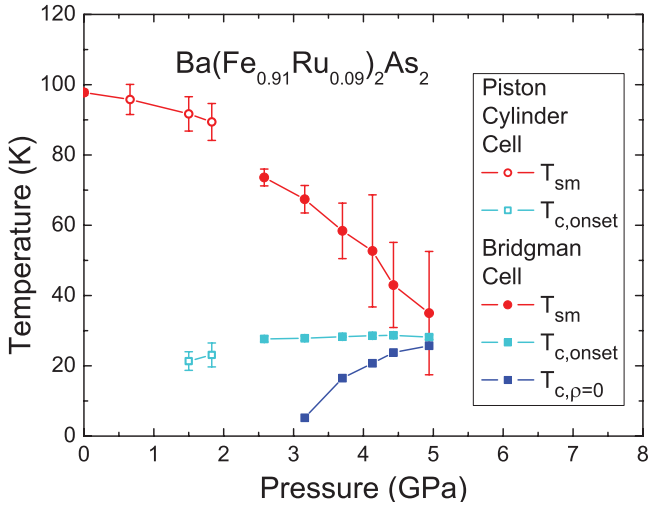

FIG. 6. (Color online) $T - P$ phase diagram for measurements of $Ba(Fe_{0.91}Ru_{0.09})_2As_2$. Open and solid symbols indicate measurements using the piston cylinder cell and the modified Bridgman cell, respectively.

and 5(d). As T_{sm} is suppressed, the minimum of $d\rho/dT$, which was used to determine T_{sm}, becomes broader and, near P_{crit}, becomes indistinguishable from the onset of T_c. The phase diagram shows a consistent qualitative behavior with T_{sm} decreasing with pressure and a superconducting T_c dome arising at higher pressures; the addition of $x = 0.09$ Ru simply shifts P_{crit} and the superconducting dome to lower pressures.

C. $Ba(Fe_{0.84}Ru_{0.16})_2As_2$

Measurements of $\rho(T, P)$ were carried out on three samples of $Ba(Fe_{0.84}Ru_{0.16})_2As_2$: one with the piston cylinder cell up to 2.30 GPa and two with the Bridgman cell with maximum pressures of 1.57 and 4.97 GPa. As shown in Fig. 1, $Ba(Fe_{0.84}Ru_{0.16})_2As_2$ also resides on the low-x side of the $T - x$ phase diagram, but with a further reduction of the structural/magnetic phase transition and much closer proximity to the superconducting dome. Ambient pressure resistivity measurement (Fig. 7) of $Ba(Fe_{0.84}Ru_{0.16})_2As_2$ shows both the structural/magnetic transition as well as the onset of superconductivity. Added pressure decreases T_{sm} and a finite $T_{c,\rho=0}$ is achieved with 1.57 GPa of pressure. A maximum $T_{c,\rho=0}$ of 23 K is achieved with 3.57 GPa, and the narrowest superconducting transition width is realized at 4.09 GPa with a $T_{c,\rho=0}$ of 22.9 K and width of $\Delta T_c \sim 0.4$ K. At 4.09 GPa the structural/magnetic transition has all but disappeared. Further pressure increase causes the structural/magnetic transition to disappear completely, a decrease in T_c, and a broadening of the superconducting transition.

For the low-pressure piston cylinder cell measurements the structural/magnetic transition at 0.5 GPa is broader than at 0.9 GPa and $T_{c,onset}$ is also higher. One possible cause of this is that the first pressurization could have caused strains in the sample due to a small increase in pressure from constrictions and contractions of the cell from the first cooling and warming of the cell. Of greater concern is the fact that there are noticeable differences between measurements done in the piston cylinder and the Bridgman cell. For the 1.53

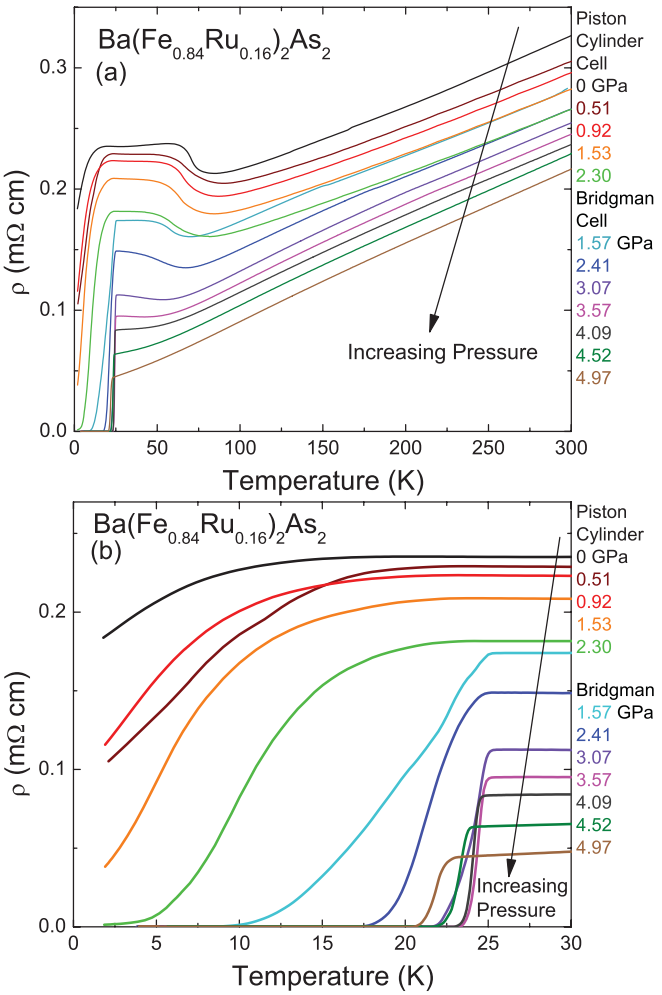

FIG. 7. (Color online) Temperature dependence of the resistivity of $Ba(Fe_{0.84}Ru_{0.16})_2As_2$ up to 2.30 and 4.97 GPa measured using the piston cylinder cell and the modified Bridgman cell, respectively. (a) Shown for temperatures up to 300 K. (b) Shown for temperatures up to 30 K.

and 2.30 GPa measurements from the piston-cylinder cell and 1.57 and 2.41 GPa measurements from the Bridgman cell, the corresponding sets of the temperature-dependent resistivity data overlap well from room temperature down to ~150 K, below which the resistivity of the sample in the Bridgman cell is suppressed much faster. Furthermore, in this pressure range the Bridgman cell measurements manifest a sharp superconducting transition, whereas for the piston cylinder cell the transition is wider and does not reach $\rho = 0$, even at the base temperature of 1.8 K. In addition, the $T_{c,onset}$ values are consistently lower in the piston cylinder cell than in the Bridgman cell, and the rate of suppression of T_{sm} is smaller in the piston cylinder cell. These differences suggest a slight disparity in the degree of hydrostaticity between the piston cylinder cell with the light mineral oil : n-pentane mixture and the Bridgman cell using the isopentane : n-pentane mixture. In the $x = 0.09$ Ru measurements, these differences were also seen, although smaller. Despite these discrepancies, the combined phase diagram shown in Fig. 8 demonstrates rather good agreement between measurements taken with these two cells.

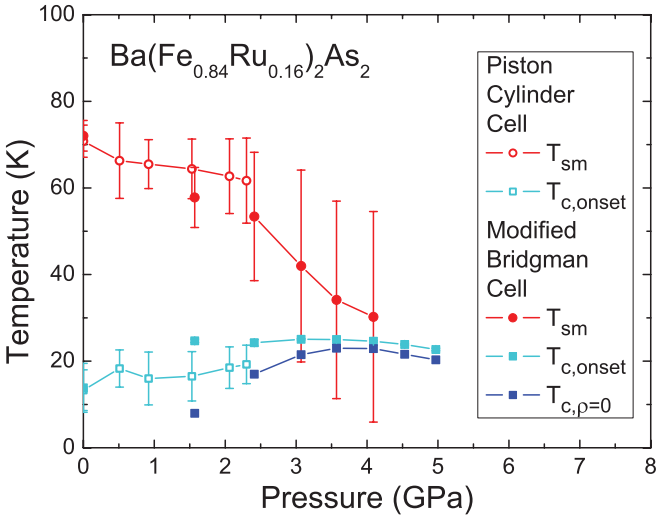

FIG. 8. (Color online) $T - P$ phase diagram for measurements of $Ba(Fe_{0.84}Ru_{0.16})_2As_2$. Open and solid symbols indicate measurements using the piston cylinder cell and the modified Bridgman cell, respectivdely.

D. $Ba(Fe_{0.79}Ru_{0.21})_2As_2$

$Ba(Fe_{0.79}Ru_{0.21})_2As_2$ is very close to the optimal Ru concentration (see Fig. 1). At higher Ru concentrations the homogeneity of the Ru substitution starts to vary within the batch of samples, as reported by Thaler *et al.*[11] Figure 9 shows the results of resistivity measurements for the samples used in the piston cylinder cell and the Bridgman cell for pressures up to 1.12 and 7.39 GPa, respectively, both using the isopentane : *n*-pentane mixture. At ambient pressure, $Ba(Fe_{0.79}Ru_{0.21})_2As_2$ samples show a coexistence of both the structural/magnetic transition and superconductivity. The ambient pressure T_c for the two samples used in the cells differs by ~1 K. A maximum $T_{c,\rho=0}$ of 20.3 K was achieved with only 2.27 GPa and also has the narrowest transition width at this pressure. Further pressure increases causes the suppression of T_c and a widening of the transition width.

The phase diagram for $Ba(Fe_{0.79}Ru_{0.21})_2As_2$ is shown in Fig. 10. T_{sm} in the piston cylinder cell ($P < 1.2$ GPa) is only weakly affected by pressure, whereas by $P = 2.27$ GPa (the first finite pressure in the Bridgman cell) T_{sm} was significantly decreased. As with other substitution levels, $T_c(P)$ forms a domelike region, with the highest and sharpest T_c found near $P_{crit} = 3.28$ GPa.

E. $Ba(Fe_{0.72}Ru_{0.28})_2As_2$

$Ba(Fe_{0.72}Ru_{0.28})_2As_2$, having optimal Ru concentration, shows no structural/magnetic transition at ambient pressure, and the superconducting transition is relatively sharp, with $T_c \sim 16$ K and the transition width $\Delta T_c \sim 0.7$ K. Added pressure marginally increases $T_{c,onset}$ and in fact widens the transition width as $T_{c,\rho=0}$ decreases, as shown in Figs. 11 and 12. The superconducting onset and zero resistivity temperatures show very little scatter compared to low-pressure measurements on the other Ru-substituted samples.

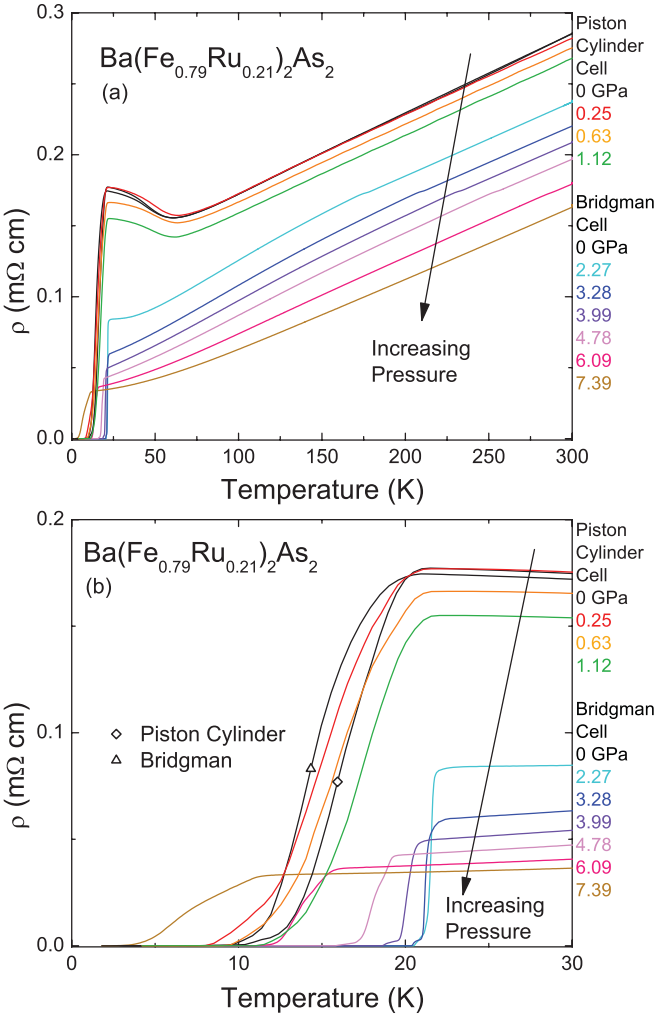

FIG. 9. (Color online) Temperature dependence of the resistivity of $Ba(Fe_{0.79}Ru_{0.21})_2As_2$ up to 1.12 and 7.39 GPa measured using the piston cylinder cell and the modified Bridgman cell, respectively. (a) Shown for temperatures up to 300 K. (b) Shown for temperatures up to 30 K.

IV. DISCUSSION

Previous pressure studies have shown that $BaFe_2As_2$ and related compounds are sensitive to the degree of nonhydrostaticity of the pressurized environment.[13–17] Empirically, increasingly hydrostatic environments move T_{sm} and T_c to higher pressures on the $T - P$ phase diagram. Having the pressure-transmitting medium still be a liquid at room temperature when pressure is increased reduces the degree of uniaxial stress on the sample. In such cases any nonhydrostaticity is caused upon cooling and warming by the differential thermal contractions of the various components of the cell below the vitrification/solidification temperature (the temperature below which the liquid medium changes into a glass or solid).

For measurements taken with the piston cylinder cell, the superconducting onsets were broader and more rounded than those taken with the Bridgman cell. This is expected since the samples for the piston cylinder cell were typically twice as long as those for the Bridgman cell. Longer samples are

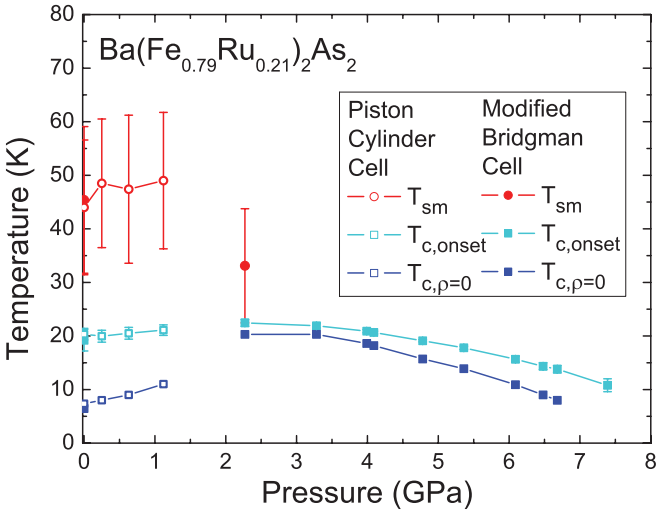

FIG. 10. (Color online) $T - P$ phase diagram for measurements of $Ba(Fe_{0.79}Ru_{0.21})_2As_2$. Open and solid symbols indicate measurements using the piston cylinder cell and the modified Bridgman cell, respectively.

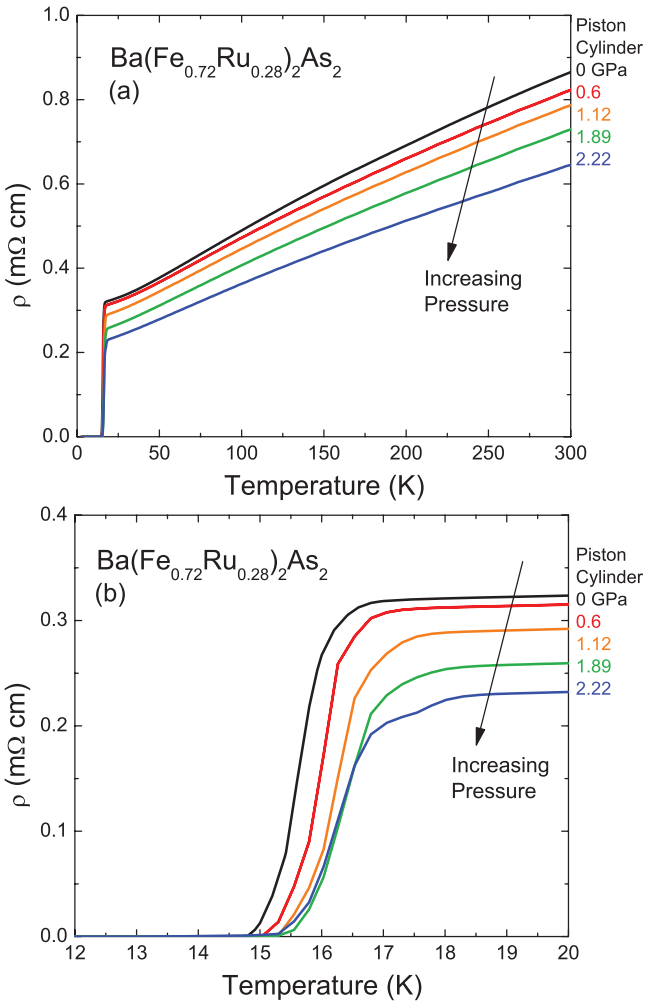

FIG. 11. (Color online) Temperature dependence of the resistivity of $Ba(Fe_{0.72}Ru_{0.28})_2As_2$ up to 2.22 GPa measured using the piston cylinder cell. (a) Shown for temperatures up to 300 K. (b) Shown for temperatures up to 20 K.

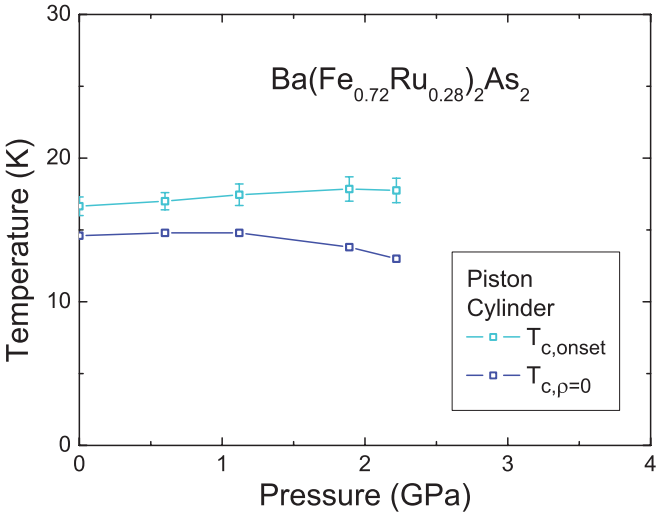

FIG. 12. (Color online) $T - P$ phase diagram for measurements of $Ba(Fe_{0.72}Ru_{0.28})_2As_2$ using the piston cylinder cell.

more vulnerable to pressure inhomogeneities due to the larger region across which strain gradients can occur.

The effect of strain gradients and or internal crystallographic strain[30] (associated with dislocation and other mechanically induced defects) on the samples can also be invoked to explain the relatively low-pressure sensitivity of the $T_{c,\text{onset}}$ line in the phase diagrams. Given that $T_{c,\rho=0}$ forms a fairly well-defined, pressure-dependent domelike region, $T_{c,\text{onset}}$ can be understood in terms of an effective strain gradient over some region of the sample, equivalent to several gigapascals. With such a gradient, a wide distribution of the T_c values could exist, leading to a fairly pressure-insensitive $T_{c,\text{onset}} \sim T_{c,\text{max}}$. This is precisely what is seen here as well as in $SrFe_2As_2$ (Ref. 30) and inferred by Nakashima *et al.*[32] Based on this premise, we pay far greater attention to the $T_{c,\rho=0}(P)$ data.

All of the $T - P$ phase diagrams for $Ba(Fe_{1-x}Ru_x)_2As_2$ are shown together in Fig. 13. Although the suppression of

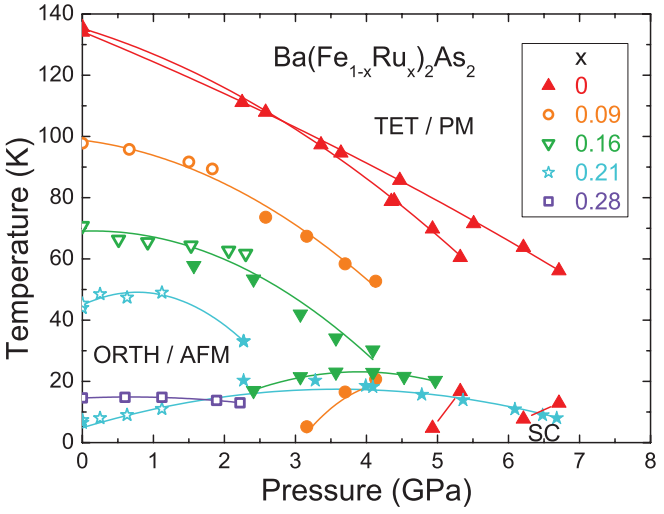

FIG. 13. (Color online) Combined phase diagram for all Ru concentrations. Open and closed symbols are transition temperatures from measurements using the piston cylinder cell and Bridgman cell, respectively. Lines are guides for the eyes.

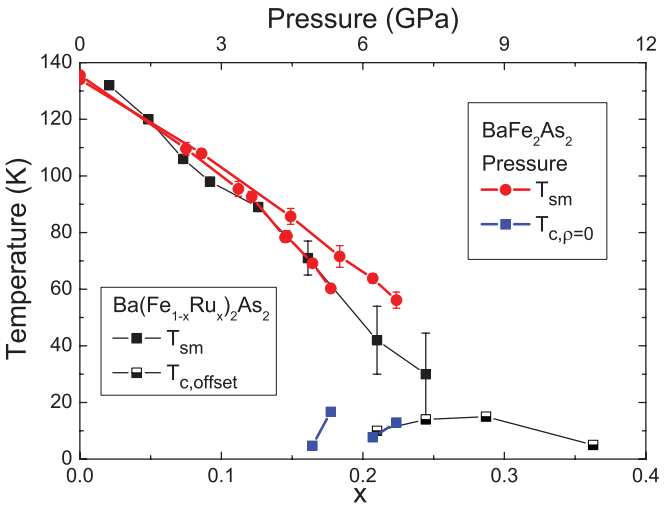

FIG. 14. (Color online) Comparison of the $T - x$ phase diagram for $Ba(Fe_{1-x}Ru_x)_2As_2$ and $T - P$ phase diagram of $BaFe_2As_2$ with a ratio of 3 GPa to $x = 0.10$ Ru relating the two horizontal axes.

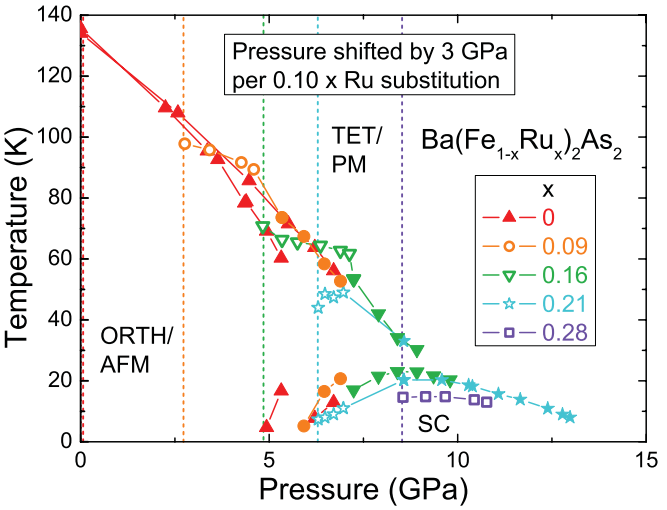

FIG. 15. (Color online) Phase diagram of all Ru concentrations each shifted by 3 GPa for every $x = 0.10$ Ru substitution. Open and closed symbols are transition temperatures from measurements using the piston cylinder cell and Bridgman cell, respectively.

T_{sm} with increasing Ru concentration and pressure is clear, as is the stabilizing of the superconducting region, this plot does not clearly reveal any other unifying trends.

In the earlier study of Ru substitution in $BaFe_2As_2$,[11] a comparison was made between the $T - x$ phase diagram and the $T - P$ phase diagram of the parent compound. We make the same comparison here, in Fig. 14, with measurements taken with the isopentane : n-pentane mixture. Although the full superconducting dome was not determined under pressure for pure $BaFe_2As_2$, by overlapping the T_{sm} suppression curve, it is readily seen that 3 GPa is grossly comparable to $x = 0.10$ Ru substitution for these pressure conditions. It should be noted that for the Fluorinert 70 : 77 pressure medium used in the Bridgman cell,[11,13] this relation was close to 2 GPa to $x = 0.10$ Ru. Clearly this relationship depends on multiple factors, most likely associated with non-hydrostatic pressure components due to the freezing of the liquid medium.

Using this relationship from pure $BaFe_2As_2$ under pressure and ambient pressure $Ba(Fe_{1-x}Ru_x)_2As_2$, a more revealing composite phase diagram can be created by shifting the $T - P$ phase diagrams for the various Ru concentrations according to the ratio 3 GPa : $x = 0.10$ Ru. When this is done (see Fig. 15), the data form a much more consistent picture, with T_{sm} and T_c manifolds lying roughly on top of each other. It is important to point out that although the pressure : Ru concentration ratio was based on T_{sm} normalization, the $T_{c,\rho=0}$ data fall onto a consistent manifold as well. Figure 15 demonstrates that for all Ru concentrations that were studied, only a single scaling, 3 GPa for $x = 0.10$ Ru, is necessary to line up the phase diagrams. This means that the effects of pressure and Ru substitution on $BaFe_2As_2$ are additive in a simple manner across the whole phase diagram. It must be emphasized, though, that this scaling value, 3 GPa $\sim 0.1\ x$ Ru, is associated with a specific pressure media. For the Fluorinert mixture used by Colombier *et al.*,[13] the scaling is 2.2 GPa $\sim 0.1\ x$ Ru, and using data from Yamazaki *et al.*,[17] a scaling of 5 GPa $\sim 0.1\ x$ Ru can be inferred.

Whereas both pressure and Ru substitution are nominally isoelectronic, a similar composite phase diagram can be assembled from $T - x - P$ data collected on $Ba(Fe_{1-x}Co_x)_2As_2$ samples.[22] In this non-isoelectronic case, a scaling of 0.8 GPa : $x = 0.01$ Co gives the best collapse of the data onto single T_{sm} and T_c manifolds. This result implies that the additive nature of doping and pressure may not be limited to isoelectronic substitutions.

Another way of seeing the effect of pressure on the $Ba(Fe_{1-x}Ru_x)_2As_2$ system is to plot the maximum $T_{c,\rho=0}$ on the ambient pressure $T - x$ phase diagram (Fig. 16). Because P_{crit} was not reached with parent $BaFe_2As_2$, with this pressure medium we use the maximum value reported by Colombier *et al.*[13] as an estimate. For the lower-than-optimal Ru-substituted samples, as pressure suppresses the structural/

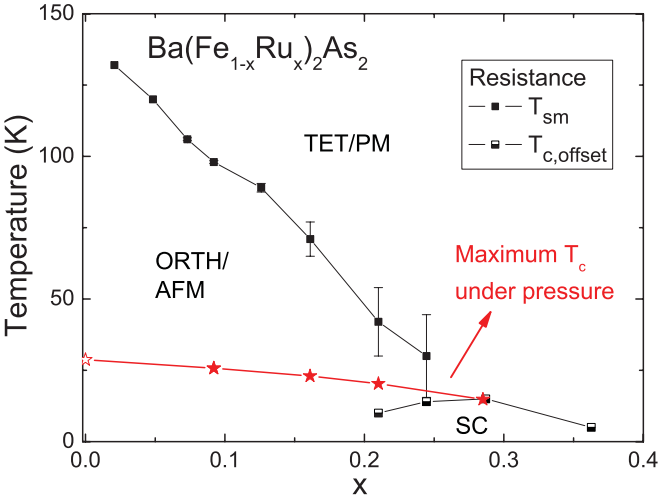

FIG. 16. (Color online) Comparison of $T - x$ phase diagram and the maximum $T_{c,\rho=0}$ achieved with pressure at various Ru concentrations. Solid stars are $T_{c,\max}$ values from this study. The open star is the $T_{c,\max}$ reported by Colombier *et al.*[13]

magnetic transition, T_c dramatically increases, as was the case for Co-substituted $BaFe_2As_2$.[22] On the other hand, if T_{sm} has already been suppressed, by either Co or Ru substitution, pressure no longer increases T_c but rather suppresses it. This is consistent with the idea that long-range structural/magnetic ordering is detrimental for superconductivity and is the primary reason T_c is low or absent in suboptimally substituted samples.

Figures 15 and 16 bring up an interesting question, perhaps a key one: Do Ru substitution and pressure produce similar phase diagrams via similar or different mechanisms? At a gross level the reason for the similarity is the same: suppression of T_{sm} leads to an increase in T_c, as has been observed for a wide range of transition metal substitutions.[1] Both Ru substitution and pressure suppress T_{sm}. The question becomes whether this is accomplished via similar or different mechanisms. Whereas it is fairly certain that pressure can change only details of the band structure (such as nesting or density of states near the fermi surface), Ru substitution may change the band structure[12] or it may suppress the magnetic transition temperature by replacing Fe with a far less magnetic ion. For example, in a simple Stoner picture, the magnetic moment can depend on a product of density of states and on-site repulsion. Ru can change both, whereas pressure will not significantly change the on-site term for Fe. In this light, Ru substitution would be a less dramatic example of substituting Y or Lu for Rare Earth = Gd–Tm in a rare earth intermetallic compound,[33] perhaps involving Stoner enhancement, rather than local moments. Ultimately, systematic studies, across the whole Ru series, via ARPES will help address these questions.

V. CONCLUSION

Pressure measurements have been carried out on the $Ba(Fe_{1-x}Ru_x)_2As_2$ system. The resulting phase diagrams show a suppression of T_{sm} and an enhancement of T_c up to P_{crit}, where we see the narrowest superconducting transition $T_{c,max}$ and the disappearance of T_{sm} by the addition of pressure for underdoped compounds. For the optimal Ru concentrations, further pressure increases beyond P_{crit} lowers T_c and broadens the superconducting transition. Comparisons between the $Ba(Fe_{1-x}Ru_x)_2As_2$ $T-x$ phase diagrams indicate an additive correlation between physical pressure and Ru substitution of 3 GPa to $x = 0.10$ Ru concentration. A comparison between $T_{c,max}$ and the $T-x$ phase diagram indicates that suppression of the structural/magnetic transition is necessary for superconductivity to reach its maximum T_c values.

ACKNOWLEDGMENTS

We thank E. D. Mun, X. Lin, and A. Kreyssig for enlightening discussions. This work was carried out at Ames Laboratory, US DOE, under Contract No. DE-AC02-07CH11358 (SKK, EC, AT, SLB, and PCC). Part of this work was performed at the Iowa State University and supported by the AFOSR-MURI, Grant No. FA9550-09-1-0603 (MST and PCC). MST was supported in part by the National Science Foundation under Grant No. DMR-0805335. S.L.B. acknowledges partial support from the State of Iowa through Iowa State University.

APPENDIX

Given the importance of hydrostaticity for the measurements of $\rho(T)$ under pressure, we opted for a pressure medium that solidifies at relatively high pressure at ambient temperature, thus reducing nonhydrostatic components associated with the pressurization process. As a side product of this study, we were able to use the sensitivity of $Ba(Fe_{1-x}Ru_x)_2As_2$ to pressure conditions to track the melting temperature of the two liquid media at various pressures. We found that upon warming the resistivity data for various pressures and samples showed a small, anomalous, kinklike feature at higher temperatures [see Fig. 17(a)]. Because this resistive anomaly consistently appeared at similar temperatures for similar pressures and was independent of Ru content, it was attributed to a subtle change in the pressure conditions. For the Bridgman cell with the 1 : 1 isopentane : *n*-pentane mixture, this feature was found to correspond to the melting temperature of the liquid medium.[34] Although this feature is essentially invisible in the $\rho(T)$ plots shown in the main text and is even difficult to

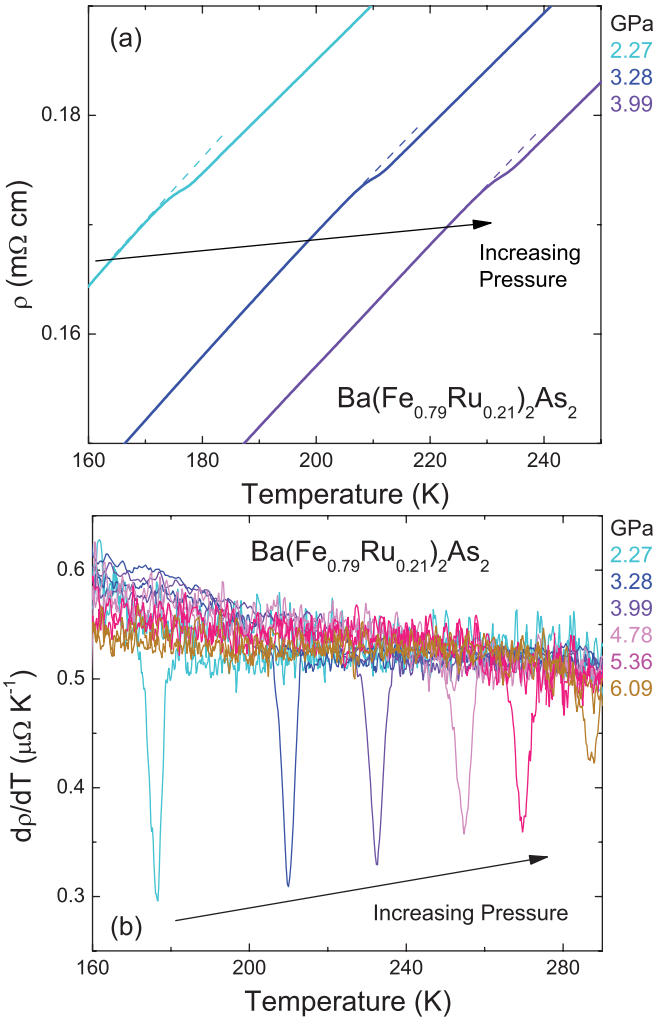

FIG. 17. (Color online) (a) Feature in resistivity data for $Ba(Fe_{0.79}Ru_{0.21})_2As_2$ at 2.27, 3.28, and 3.99 GPa. Dashed are extrapolations of the lower temperature, linear $\rho(T)$ data. (b) Feature in $d\rho/dT$ indicative of the melting of the liquid medium.

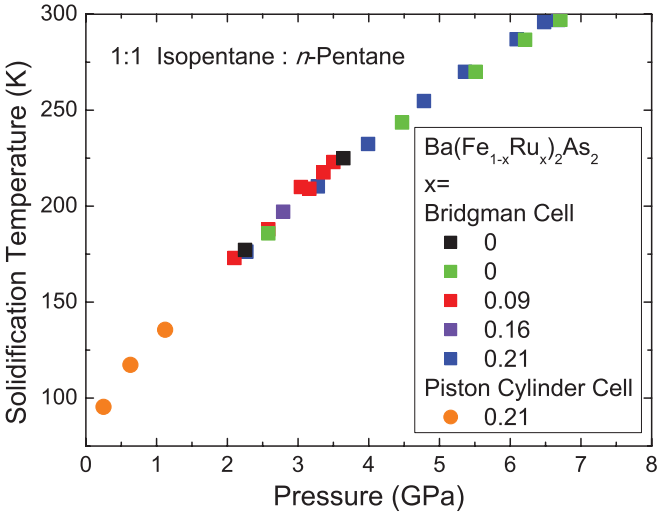

FIG. 18. (Color online) Combined phase diagram of the melting of the liquid medium (1 : 1 isopentane : *n*-pentane).

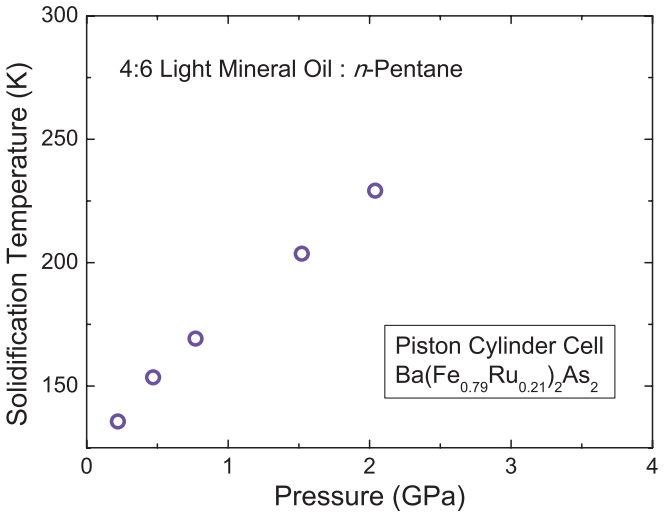

FIG. 19. (Color online) Combined phase diagram of the melting of the liquid medium 4 : 6 light mineral oil : *n*-pentane.

see in the expanded Fig. 17(a), this feature is readily seen in the derivative of the resistivity, Fig. 17(b). The minimum of this derivative was taken as the vitrification/solidification temperature of the liquid medium.

The $T - P$ phase diagram inferred from these data is presented in Fig. 18. When this curve is extrapolated to zero pressure, the melting event occurs at ∼85 K. This is lower than the previously reported freezing temperatures (105 K and 125 K at ambient pressure[34,35]), but this discrepancy is not unexpected given the different criterion used to determine the solidification temperature. Sundqvist[35] measured the resistivity of a Manganin wire suspended in this liquid medium and noted the temperature at which the resistivity dramatically diverges from the expected linear behavior, indicating the onset of solidification. On the other hand, Klotz *et al.*[34] used the "blocked-capillary method," where a thin capillary inside a temperature-controlled copper block is filled with the liquid medium. In this case the reported values were for temperatures where the liquid medium attains a viscosity similar to thick molasses.

More importantly, it is useful to know the hydrostatic limit of the liquid medium at the temperature when pressure is applied. Usually this is at room temperature (∼300 K). Both Piermarini *et al.*[27] and Klotz *et al.*[29] placed rubies in a diamond anvil cell filled with the isopentane and *n*-pentane mixture. At 7.4 GPa they saw a broadening of the spectral line of rubies that could be correlated to the solidification of the medium. The hardness of rubies makes them less sensitive to pressure gradients; therefore 7.4 GPa can be considered a higher hydrostatic limit of the liquid medium. A different approach was used by Nomura *et al.*,[36] where, once again, the resistivity of a Manganin wire was suspended in the liquid medium, but this time inside a cubic anvil pressure cell. At 283 K the resistivity of the Manganin wire diverged from the expected linear behavior at 5.6 GPa.[36]

In our study the anomaly seen in the resistivity curves indicate that the melting event occurs at ∼6.5 GPa at 300 K, which is within the range of previously reported values. In fact, at ∼283 K, the hydrostatic limit from our study is 6.0 GPa, which is only 0.4 GPa higher than the results from Nomura *et al.*[36]

The advantage of this study was that the freezing transition was tracked across a wide range of temperatures and pressures. Previous reports[27,29,34,36] on the vitrification/solidification of the isopentane : *n*-pentane mixture were typically studied only at a given temperature or pressure.

In a similar manner, the vitrification/solidification temperature of the 4 : 6 light mineral oil : *n*-pentane mixture was determined at several pressures using the piston cylinder cell. The resistivity data for $Ba(Fe_{0.79}Ru_{0.21})_2As_2$ taken upon warming with this liquid medium showed a similar anomalous kink; the derivative of the resistivity data showed a clear feature that we took to be the vitrification/solidification event. Figure 19 shows the $T - P$ phase diagram for this liquid medium. At 300 K this phase transition is expected to occur at a pressure of roughly 3.5 GPa, thus quantitatively justifying the use of this liquid medium at pressures up to 3 GPa in the past.[37]

[1]P. C. Canfield and S. L. Bud'ko, Annu. Rev. Condens. Matter Phys. **1**, 27 (2010).
[2]M. Rotter, M. Tegel, and D. Johrendt, Phys. Rev. Lett. **101**, 107006 (2008).
[3]M. Rotter, C. Hieke, and D. Johrendt, Phys. Rev. B **82**, 014513 (2010).
[4]S. Kasahara, T. Shibauchi, K. Hashimoto, K. Ikada, S. Tonegawa, R. Okazaki, H. Shishido, H. Ikeda, H. Takeya, K. Hirata, T. Terashima, and Y. Matsuda, Phys. Rev. B **81**, 184519 (2010).
[5]M. G. Kim, A. Kreyssig, A. Thaler, D. K. Pratt, W. Tian, J. L. Zarestky, M. A. Green, S. L. Bud'ko, P. C. Canfield, R. J. McQueeney, and A. I. Goldman, Phys. Rev. B **82**, 220503 (2010).

[6]N. Ni, M. E. Tillman, J. Q. Yan, A. Kracher, S. T. Hannahs, S. L. Bud'ko, and P. C. Canfield, Phys. Rev. B **78**, 214515 (2008).
[7]N. Ni, A. Thaler, J. Q. Yan, A. Kracher, E. Colombier, S. L. Bud'ko, P. C. Canfield, and S. T. Hannahs, Phys. Rev. B **82**, 024519 (2010).
[8]A. S. Sefat, R. Jin, M. A. McGuire, B. C. Sales, D. J. Singh, and D. Mandrus, Phys. Rev. Lett. **101**, 117004 (2008).
[9]A. S. Sefat, D. J. Singh, L. H. VanBebber, Y. Mozharivskyj, M. A. McGuire, R. Jin, B. C. Sales, V. Keppens, and D. Mandrus, Phys. Rev. B **79**, 224524 (2009).
[10]J.-H. Chu, J. G. Analytis, C. Kucharczyk, and I. R. Fisher, Phys. Rev. B **79**, 014506 (2009).
[11]A. Thaler, N. Ni, A. Kracher, J. Q. Yan, S. L. Bud'ko, and P. C. Canfield, Phys. Rev. B **82**, 014534 (2010).
[12]F. Rullier-Albenque, D. Colson, A. Forget, P. Thuéry, and S. Poissonnet, Phys. Rev. B **81**, 224503 (2010).
[13]E. Colombier, S. L. Bud'ko, N. Ni, and P. C. Canfield, Phys. Rev. B **79**, 224518 (2009).
[14]K. Matsubayashi, N. Katayama, K. Ohgushi, A. Yamada, K. Munakata, T. Matsumoto, and Y. Uwatoko, J. Phys. Soc. Jpn. **78**, 073706 (2009).
[15]F. Ishikawa, N. Eguchi, M. Kodama, K. Fujimaki, M. Einaga, A. Ohmura, A. Nakayama, A. Mitsuda, and Y. Yamada, Phys. Rev. B **79**, 172506 (2009).
[16]W. J. Duncan, O. P. Welzel, C. Harrison, X. F. Wang, X. H. Chen, F. M. Grosche, and P. G. Niklowitz, J. Phys. Condens. Matter **22**, 052201 (2010).
[17]T. Yamazaki, N. Takeshita, R. Kobayashi, H. Fukazawa, Y. Kohori, K. Kihou, C. H. Lee, H. Kito, A. Iyo, and H. Eisaki, Phys. Rev. B **81**, 224511 (2010).
[18]M. S. Torikachvili, S. L. Bud'ko, N. Ni, and P. C. Canfield, Phys. Rev. B **78**, 104527 (2008).
[19]M. S. Torikachvili, S. L. Bud'ko, N. Ni, and P. C. Canfield, Phys. Rev. Lett. **101**, 057006 (2008).
[20]P. L. Alireza, Y. T. C. Ko, J. Gillett, C. M. Petrone, J. M. Cole, G. G. Lonzarich, and S. E. Sebastian, J. Phys. Condens. Matter **21**, 012208 (2009).
[21]H. Kotegawa, T. Kawazoe, H. Sugawara, K. Murata, and H. Tou, J. Phys. Soc. Jpn. **78**, 083702 (2009).
[22]E. Colombier, M. S. Torikachvili, N. Ni, A. Thaler, S. L. Bud'ko, and P. C. Canfield, Supercond. Sci. Technol. **23**, 054003 (2010).
[23]S. A. J. Kimber, A. Kreyssig, Y.-Z. Zhang, H. O. Jeschke, R. Valent, F. Yokaichiya, E. Colombier, J. Yan, T. C. Hansen, T. Chatterji, R. J. McQueeney, P. C. Canfield, A. I. Goldman, and D. N. Argyriou, Nat. Mater. **8**, 471 (2009).
[24]E. Colombier and D. Braithwaite, Rev. Sci. Instrum. **78**, 093903 (2007).
[25]A. Eiling and J. S. Schilling, J. Phys. F **11**, 623 (1981).
[26]V. A. Sidorov and R. A. Sadykov, J. Phys. Condens. Matter **17**, S3005 (2005).
[27]G. J. Piermarini, S. Block, and J. D. Barnett, J. Appl. Phys. **44**, 12 (1973).
[28]T. Sakai, T. Kagayama, and G. Oomi, J. Mater. Process. Technol. **85**, 224 (1999).
[29]S. Klotz, J.-C. Chervin, P. Munsch, and G. Le Marchand, J. Phys. D **42**, 075413 (2009).
[30]S. R. Saha, N. P. Butch, K. Kirshenbaum, J. Paglione, and P. Y. Zavalij, Phys. Rev. Lett. **103**, 037005 (2009).
[31]R. Hu, S. L. Bud'ko, W. E. Straszheim, and P. C. Canfield, Phys. Rev. B **83**, 094520 (2011).
[32]Y. Nakashima, H. Yui, and T. Sasagawa, Physica C **470**, 1063 (2010).
[33]T. A. Wiener, I. R. Fisher, S. L. Bud'ko, A. Kracher, and P. C. Canfield, Phys. Rev. B **62**, 15056 (2000).
[34]S. Klotz, J. Philippe, and E. Cochard, J. Phys. D **39**, 1674 (2006).
[35]B. Sundqvist, J. Phys. E **20**, 984 (1987).
[36]M. Nomura, T. Nishizaka, Y. Hirata, N. Nakagiri, and H. Fujiwara, Jpn. J. Appl. Phys. **21**, 936 (1982).
[37]S. L. Bud'ko, A. N. Voronovskii, A. G. Gapotchenko, and E. S. Itskevich, Zh. Eksp. Teor. Fiz. **86**, 778 (1984).